Received: 1 March 2019 | Revised: 23 July 2019 | Accepted: 25 August 2019

DOI: 10.1002/htj.21583

HEAT TRANSFER
Asian Research

WILEY

ORIGINAL ARTICLE

The effect of a periodic tangential magnetic field on the stability of a horizontal magnetic fluid sheet

Galal M. Moatimid[1] | **Nabil T. Eldabe**[1] | **Aya Sayed**[2]

[1]Department of Mathematics, Faculty of Education, Ain Shams University, Cairo, Egypt

[2]Department of Mathematics and Computer Science, Faculty of Science, Beni-Suef University, Beni-Suef, Egypt

Correspondence
Aya Sayed, Department of Mathematics and Computer Science, Faculty of Science, Beni-Suef University, Beni-Suef, Egypt.
Email: Aya.Sayed@science.bsu.edu.eg

Abstract

The current article aims at investigating the effect of a periodic tangential magnetic field on the stability of a horizontal flat sheet. The media were considered porous, the three viscous-fluid layers were initially streaming with uniform velocities, and the magnetic field admitted the presence of free-surface currents. Furthermore, the transfer of mass and heat phenomenon was taken into account. The analysis, in this paper, was followed by the viscous potential theory. Moreover, the stability of the boundary-value problem resulted in coupled second-order linear differential equations with damping and complex coefficients. In regard to the uniform and periodic magnetic field, the standard normal mode approach was applied to deduce a general dispersion relation and judge the stability criteria. In addition, several unfamiliar cases were reported, according to appropriate data choices. The stability conditions were theoretically analyzed, and the influences of the various parameters in the stability profile were identified through a set of diagrams. In accordance wth the oscillating field, the coupled dispersion equations were combined to give the established Mathieu equation. Therefore, the governed transition curves were, theoretically, obtained. Finally, the results were numerically confirmed.

KEYWORDS
magnetic field, mass and heat transfer, porous media, stability analysis, viscous potential flow

1 | INTRODUCTION

Rayleigh-Taylor instability (RTI) occurs when, with reference to density, a dense fluid is pushed by a lighter one. Due to the wide range of applications of RTI in planetary and stellar atmospheres, as well as other fields, it has been addressed in several studies. This phenomenon was first investigated by Rayleigh,[1] and then later by Taylor[2] who showed that, when two superposed fluids of different densities are accelerated in a direction perpendicular to their interface, the surface becomes stable or unstable according to whether the acceleration is directed from the heaviest to lighter fluid or vice versa. There are two streams of research that investigated this phenomenon: physics and engineering. A significant review of the hydrodynamic stability for RTI and Kelvin-Helmholtz instability (KHI) has been reported throughout Chandrasekhar's[3] pioneering book. El-Shehawey et al.[4] studied the electrohydrodynamic stability of a fluid layer that imbedded between two different fluids. Their inviscid fluid system was influenced, only, by the gravitational forces together with the tangential electric field. They showed that the tangential electric field plays a stabilizing role, it may be used to suppress the instability of the system at a certain wave number. The stability analysis resulted in two simultaneous linear second-order differential equations. The current study involved many parameters, unlike previous studies. Mohamed et al.[5] introduced the same problem that was given by El-Shehawey et al.[4] but in case of a periodic electric field. In this case, they obtained two simultaneous ordinary differential equations of the Mathieu type. They used the multiple time scale technique to judge the stability criteria. They showed that the tangential periodic field cannot stabilize a system that is unstable under a uniform electric field. Actually, the current paper includes the behavior of the fields that was given by El-Shehawey et al.[4] and Mohamed et al.[5] Mohamed et al.[6] studied the elecrohydrodynamic of two interfaces separating three fluid phases. They considered two cases: the case of the absence of the surface charges together with that in their presence. They showed that the field still has a destabilizing influence, but this influence is partially shielded in some situations. Similar influence has been considered in the current paper as the tangential admitted the presence of free-surface currents at the interface. El-Dib and Matoog[7] investigated the problem by electroviscoelastic Kelvin-Helmholtz waves of three-phase Maxwellian fluids under the influence of a periodic orthogonal electric field in the absence of surface charges. They used the symmetric and antisymmetric modes in their analysis. Moreover, they indicated that the thickness of the horizontal layer as well as the frequency of the layer played a destabilizing role in the stability picture. Similar analysis as that given by El-Dib and Matoog[7] has been utilized in the current paper. Recently, Moatimid et al.[8] investigated the influence of an axial periodic field on streaming flows throughout three coaxial infinite cylinders. The latter study is more relevance to the current study in considering the viscous potential theory as well as the porous media.

In the literature, magnetic fluids are referred to as ferromagnetic fluids or simply, ferrofluids. The study of magnetic fluids is critical due to its application in the industry, for instance, design of sprays and inkjet printers. Many researchers have studied the magnetohydrodynamic stability problems such as, linear stability of a ferrofluid on a rigid horizontal plane under a tangential magnetic field, as was investigated by Zelazo and Melcher.[9] In addition, the effect of capillary-gravity waves at the

surface of separation between two unbounded magnetic fluids in permeable media was studied by El-Dib.[10] In addition, Elhefnawy et al.[11] examined the nonlinear stability of two-phase magnetic fluids in permeable media under the action of a constant normal magnetic field. Furthermore, Alkharashi[12] deliberated a linear stability of three viscous-fluid layers in permeable media under the application of a normal magnetic field, which is normal to the surface of separation. Recently, Horstmann et al.[13] introduced a novel on-the-interface wave experiment to measure the wave amplitudes in cylindrical containers. Meanwhile, Wang[14] considered the dynamics of double incompressible electrically conducting fluid layers in the presence of a magnetic field. He showed that the viscous and nonresistive problem around the equilibrium, in the nonlinear point of view, is stable under a certain criterion.

In multiphase flows, the phenomenon of heat and mass transfer has received wider importance due to its extensive use in several fields, such as heat transfer in engineering and in geophysical applications.[15] The assumption that the fluids are immiscible is the main aspect in many studies on interface instability. Accordingly, there is no mass transfer throughout the interface. When the thermal effects are minor, it is advisable to treat the fluids as immiscible; otherwise, when there is a strong temperature gradient in the fluid, thermal influences on the interface waves must be included.[16] Consequently, mass transfer throughout the interface is of great significance. The behavior of heat and mass transfer through an interface is highly essential in a large number of industrial and environmental processes, which may comprise the design of many kinds of contacting equipment, for instance, evaporators, chemical reactors, boilers, gas absorbers, condensers, pipelines, nuclear reactors, and many others. Hsieh[17,18] is considered as the first who made a simplified formulation of the model of the interface instability in the presence of mass and heat transfer. His modeling mainly focused on the issues concerning RTI and KHI. To the best of the researchers' knowledge, Moatimid[19] extended the previous works of Hsieh[17,18] to modulate the problem of double interfaces in case of KHI. Throughout his linear analysis, he obtained coupled second-order differential equations, which had complex and periodic coefficients. To minimize the mathematical manipulations, he considered the symmetric and antisymmetric disturbances. Furthermore, Moatimid et al.[20] investigated the influences of suction and injection at the boundaries of two-phase fluids. Moreover, they studied the influence of the normal streaming velocity on the interface instability. Their study was conducted using a nonlinear stability approach. Furthermore, Awasthi[21] examined the effect of an axial electric field on the stability analysis in the presence of gravity, heat, and mass transfer. He noticed that the axial electric field suppresses the amplitudes of disturbance waves. Recently, El-Sayed et al.[22] investigated the stability analysis of the interface between two dielectric layers with interface mass and heat transfer in case of RTI. Their linear stability analysis revealed that this transfer had no implication in the stability criteria. In contrast, the nonlinear stability technique showed that it has a dual role in the stability picture. However, in the present paper, the linear approach showed an influence of the transfer of mass and heat transfer on the stability configuration.

Bau[23] investigated the stability analysis of a flat interface between two fluid layers saturated in porous media, where he derived the marginal stability criteria for the Darcian and nonDarcian fluids. Furthermore, in both cases, the instability occurs provided that the velocities should exceed some critical value. Zakaria et al.[24] studied the stability diagram of streaming magnetic fluids throughout porous media. Their model consisted of three incompressible magnetic fluid layers. They showed that the thickness of the middle layer plays a destabilizing role. In addition, dual roles were found due to the initial streaming and the porosity in the stability picture. Alkharashi and Gamiel[25] investigated the interface stability of three fluid layers, which were fully saturated in porous media. Their linearized linear stability approach

leads to two coupled Mathieu equations, where they found that the porosity had a dual influence on the stability picture. Recently, Moatimid et al.[8] investigated the influence of an axial periodic field on streaming flows throughout three coaxial infinite cylinders. The three fluids were saturated in fully saturated porous media; however, they did not consider the symmetric and antisymmetric modes in their analysis. Furthermore, the numerical calculations indicate that the coefficients of mass and heat transfers as well as the streaming play a destabilizing role, in contrast to the having a stabilizing influence. Recently, Moatimid et al.[26] introduced a few representatives of porous media in the problem of a streaming cylindrical sheet. Their analysis resulted in a damped differential equation with complex coefficients. These equations were combined to obtain a single dispersion equation. They showed that Darcy's coefficients as well as the dielectric constants played a stabilizing role in the stability picture.

Viscous potential flow received a considerable interest in numerous problems in hydrodynamic stability problems. Throughout this theory, the viscosity is ignored in the Navier-Stokes equation; simultaneously, appears only at the boundary between the two-phase fluids. It is worth noting that the theory was primarily introduced by Stokes.[27] A distinguished review on this topic was demonstrated, later, by Joseph,[28] who showed that for the potential flow $\underline{v} = -\nabla\varphi$, in case of an incompressible fluid, the solution of the Navier-Stokes equation at which the vorticity is identically zero; therefore, the term $\mu\ \nabla^2\underline{v}$ vanishes from the bulk of the fluid. Meanwhile, the viscosity occurred only at the interface. Sirwah[29] studied the interface instability between two fluids, utilizing the viscous potential theory in his approach. Furthermore, he gave numerous examples to indicate the effects of the various parameters on the stability configuration. Awasthi et al,[30] also studied the viscous corrections of the potential flow analysis of KHI of two viscous fluids in the presence of a tangential magnetic field. They demonstrated that the irrotational shearing stresses have a stabilizing effect in the presence of heat and mass transfer throughout the interface. In addition, AlHamdan and Alkharashi[31] discussed the problem of the stability characterization of three permeable layer models under a magnetic field. In this study, they ignored the stability analysis of a uniform streaming. However, unfortunately, their stability analysis for the periodic field needs more adjustment; for instance, their dispersion relationship gives a quartic equation in the frequency of the surface waves. It is of a complex nature; therefore, it has four complex roots, and they are not necessarily of complex conjugates. As a result, the zero-order solution is, exactly, unstable; consequently, there is a great doubt in their stability analysis. In contrast, the current paper gives, in more depth, the stability analysis of a uniform streaming, uniform and periodic magnetic field. A set of diagrams is given to illustrate the influence of the several parameters in the instability picture. Recently, Moatimid et al.[26] studied the influence of a uniform axial electric field on a cylindrical streaming sheet. To avoid the mathematical manipulation; their analysis was based on the viscous potential theory. Several special cases are reported upon appropriate data selections.

As a consequence of the superposed magnetic fluids, Parekh and Upadhyay[32] characterized two different magnetic fluids synthesized earlier with transformer oil as a carrier liquid. They compared the magnetic properties with those of pure transformer oil. Yayla et al.[33] gave a numerical performance to understand a two-phase flow phenomenon in coalescing or corrugating plate separators. Their study focused on the separation of water from an oil-water mixture. Chakrabarti and Das[34] studied, in detail, the three-layer flow pattern that occurs during the concurrent flow of two immiscible fluids. Therefore, the present study investigated the influence of a tangential periodic magnetic field on a fluid sheet embedded between two finite layers. Simultaneously, the magnetic field admits the presence of surface currents at the interfaces. In addition, the porous media, transfer of mass and heat, gravitational forces,

and surface tension were taken into consideration. To make a mathematical simplification, the viscous potential flow theory was utilized. The problem is significantly crucial from the geophysical perspective. This study was an extension of previous one[19] to include all of these aspects. A general dispersion relation was obtained by using the standard normal mode analysis. The stability of the system was analytically and numerically investigated. The results illustrate the interest of the fluid dynamic aspects of aquifer depletion, in petroleum stores, spray coating procedure, and metal powder manufacturing. The plan of the current work is as follows: Section 2 is devoted to introducing the mathematical formulation of the problem and the corresponding governing equations. Section 3 presents a formulation of general dispersion equations. In addition, the mathematical manipulation of these equations, from the point of view of the symmetric and antisymmetric disturbances was also presented. The stability analysis of the uniform magnetic field is depicted in Section 4. The case of the periodic field was introduced in Section 5. Finally, the concluding remarks were aew in Section 6.

2 | FORMULATION OF THE PROBLEM

The present model was confined to two horizontal, flat, rigid boundaries with the distance $2b$ apart. A magnetic infinite long horizontal liquid sheet was of finite thickness $2a$ and embedded between two other finite layers of thickness $|b - a|$. Both the viscous incompressible fluids were obtained durig uniform streaming. Furthermore, tangential periodic tangential magnetic fields were acted upon in the three layers. In addition, free-surface currents were assumed to be present at the interfaces between the three fluid layers. Consequently, the tangential magnetic field intensities must be of different strengths. Only two dimensional disturbances were considered to avoid any generality loss. For more convenience, the Cartesian coordinates (x, y) were considered; such configurations are of relevance with astrophysics and extraction of petroleum.

Figure 1 gives a full illustration of the considered system, where the horizontal x-axis is located at the center of the middle sheet. Moreover, the vertical y-axis was directed upward. The gravitational forces (g) were taken into consideration, which operate along the negative y-direction. Two undisturbed surfaces of separation between the two liquids were considered, which were taken as the initial flat to form the planes $y = -a$ and $y = a$. Within each region, all liquids were assumed to be homogeneous and saturated in porous media; therefore, the structure of the liquids was defined accoring to the following parameters; density ρ, dynamic viscosity η, the magnetic permeability μ, Darcy's coefficient ν, porosity m, periodic tangential

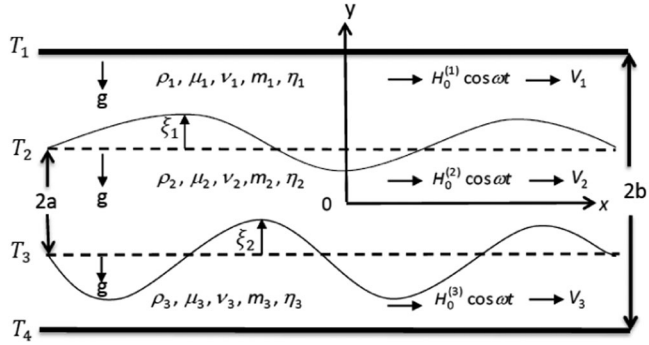

FIGURE 1 The physical model

magnetic field $H\cos\omega t$, and the streaming V. Generally, the subscripts $j = 1,\ 2$, and 3 refer to quantities in the upper, middle, and lower fluids, respectively. The mass was allowed to be transferred across the interfaces only; consequently, the immiscibility conditions no longer hold. The temperatures at the boundaries: $y = b,\ y = a,\ y = -a$, and $y = -b$ were denoted by $T_1,\ T_2,\ T_3$, and T_4, respectively. Realistically, since the transfer of mass across the interface represents a transformation of the fluid from one phase to another, there is invariably a latent heat associated with the phase change. It is essential throughout this interface coupling between the mass transfer and the release of latent heat that the motion of fluids is influenced by the thermal effects. Consequently, when there is significant mass transfer across the interface, the transfer of heat in the fluid has to be taken into consideration.

Finally, the following configuration represents a simplified formulation of the problem of stability of mass and heat transfer, which was based on a careful investigation of the previous comprehensive analysis that were given by Hsieh.[17,18]

After a limited, but a finite departure from the initial configuration, the surface deflections are expressed by considering the standard normal mode analysis,[3] the surface deflections $\xi_l(x;\ t)$ may be represented as a sinusoidal wave of finite amplitude where, after disturbance, the interface is as follows:

$$y(x;\ t) = (-)^{l+1}a + \xi_l(x;\ t) \tag{1}$$

and

$$\xi_l(x;\ t)\ = \gamma_l(t)\,\mathrm{e}^{ikx} + c.c.,\ l = 1, 2, \tag{2}$$

where $\gamma_l(t)$ is an arbitrary time-dependent function. It gives the performance of the amplitude of the disturbance at the separation surfaces, k is the wave number which is supposedly genuine and positive, while *c.c.* represents the complex conjugate of the preceding term.

It is convenient to determine the outward unit normal vectors to the interfaces, which may be obtained from the relation: $\hat{n}_l = \nabla S_l/|\nabla S_l|$, where $S_l(x, y;\ t)$ represents the surface geometry of the interfaces, which is defined as $S_l = y - (-)^{l-1}a - \xi_l(x;\ t)$.

Therefore, one gets

$$\widehat{n_l} = -\frac{\partial \xi_l}{\partial x}\underline{e}_x + \underline{e}_y, \tag{3}$$

where $\underline{e}_x$ and $\underline{e}_y$ are the unit vectors along the x- and y-directions, respectively.

Typically, as shown by Joseph[28] and others, who showed that for the potential flow $\underline{v} = -\nabla\varphi$ is, in case of an incompressible fluid, the Navier-Stokes equation behaves like the Euler's one; therefore, the term $\mu\nabla^2\underline{v}$ vanishes from the bulk of the fluid. Subsequently, the equation that governs the behavior of the viscous incompressible fluid, in case of the potential flow, throughout the permeable media, according to Brinkman-Darcy equation is given by

$$\frac{\rho_j}{m_j}\left(\frac{\partial \underline{v}_j}{\partial \mathrm{t}} + \frac{1}{m_j}(\underline{v}_j\,.\,\nabla)\underline{v}_j\right) = -\nabla P_j - \frac{\upsilon_j}{m_j}\underline{v}_j - \rho_j\, g\ \underline{e}_y, \tag{4}$$

where P_j represents the pressure in each medium.

The frictional forces are the result of the interaction force between the fluid and the permeable medium. It is proportional to the flow velocity which is represented by the term $\upsilon_j \underline{v}_j/m_j$, where $\upsilon_j = \eta_j/q_j$ is the Darcy's coefficient, η_j is the fluid viscosity, and q_j is the permeability of the porous medium.

In accordance with the simplification of the viscous potential theory, as stated above in the fifth paragraph of the introduction, the viscosity occurs only at the interfaces. Otherwise, in the bulk of the three fluids, the flows are regarded as ideal ones. Therefore, the fluids may be considered as irrotational liquids and then they their potentials obey the Laplace equation. Consequently, the standard fluid velocity rises and permitted to produce a scalar potential $\varphi(x, y; t)$, such that

$$\underline{v}_j = V_j \underline{e}_x + \nabla\varphi_j, \ j = 1, 2, 3. \tag{5}$$

Since the three fluid layers were assumed to be incompressible, the scalar potential $\varphi\ (x, y; t)$ becomes a harmonic function, that is,

$$\nabla^2\varphi_j = 0. \tag{6}$$

Typically, as in many studies on the interfacial instabilities, some of the reductions of the Maxwell's equations were satisfied to describe of hydromagnetic phenomena of the fluid system. Therefore, the quasistatic approximation[35] was usually considered. Since all fluids were subjected to horizontal magnetic fields $H_0^{(1)}$, $H_0^{(2)}$, and $H_0^{(3)}$, in which $H_0^{(1)} \neq H_0^{(2)} \neq H_0^{(3)}$. Therefore, Maxwell equations were reduced to

$$\nabla.\ (\mu_j\ \underline{H}_j) = 0 \tag{7}$$

and

$$\nabla \wedge \underline{H}_j = \underline{J}_f, \tag{8}$$

where $\underline{J}_f$ is the surface current density.

Hence, the magnetic field may be written as

$$\underline{H}_j = H_0^{(j)} \cos\omega\ t\ \underline{e}_x - \nabla\psi_j, \tag{9}$$

where $\psi_j(x, y; t)$ is a scalar function that represents the magnetic potential. It is quite clear that the stream function $\psi_j(x, y; t)$ guarantees that Equation (7) was satisfied, while the left bulk equation ($\nabla \times \underline{H}_j = \underline{0}$), indicates that the function ψ_j satisfies Laplace's equation

$$\nabla^2\psi_j = 0. \tag{10}$$

In accordance with the standard modes analysis,[3] the magnetic potential and the velocity potential may be written in the form

$$\psi_j(x, y; t) = \widehat{\psi_j}(y; t)e^{ikx} + c.c. \tag{11}$$

and

$$\varphi_j(x, y; t) = \hat{\varphi}_j(y; t)\, e^{ikx} + c.c. \tag{12}$$

Hence, the solutions of the linearized equations (6) and (10) are given by

$$\varphi_j(x, y; t) = [A_j(t)\cosh ky + B_j(t)\sinh ky]e^{ikx} + c.c. \tag{13}$$

and

$$\psi_j(x, y; t) = [C_j(t)\cosh ky + D_j(t)\sinh ky]e^{ikx} + c.c. \tag{14}$$

As a result of perturbation, the zero order of the pressure may be written as

$$P_{0j} = -\upsilon_j V_j x/m_j - \rho_j\, g\, y + \lambda_j(t), \tag{15}$$

where $\lambda_j(t)$ is an arbitrary time-dependent function.

As shown later, the continuity of the normal stresses in the zero order at the interface yields

$$\begin{aligned}\lambda_l(t) - \lambda_{l+1}(t) = (-)^{l+1}(\rho_l - \rho_{l+1})ga + (\upsilon_l V_l/m_l - \upsilon_{l+1}V_{l+1}/m_{l+1})x \\ - \frac{1}{2}\left(\mu_l H_l^2 - \mu_{l+1}H_{l+1}^2\right)\cos^2\omega t.\end{aligned} \tag{16}$$

The pressure in the first order may be evaluated from the Bernoulli's equation. In other words, the integration of the equation of motion Equation (4) yields

$$P_j(x, y; t) = -\frac{1}{k\, m_j}\left[\rho_j\left(\frac{d}{dt} + i\frac{kV_j}{m_j}\right) + \nu_j\right][A_j(t)\sinh ky + B_j(t)\cosh ky]e^{ikx} + c.c., \tag{17}$$

where $A_j(t)$, $B_j(t)$, $C_j(t)$, and $D_j(t)$ are arbitrary functions of time, which are indicated by the employment of the suitable boundary conditions

2.1 | Boundary conditions

To complete the boundary-value problem, the general potentials φ_j and ψ_j as given in Equations (13) and (14) must be specified. Therefore, it is crucial to determine the arbitrary time-dependent functions that appear in these equations. For the purpose of specifying these unknown functions, it is convenient to identify two types of boundaries: the first is that at the surface between a fluid and a rigid surface, and the second is in the fluid/fluid interfaces. Subsequently, the boundary conditions may be formulated as follows:

For the hydrodynamic path:

The related boundary conditions are illustrated, in detail, as given by Moatimid.[19] In accordance with these conditions, the following solutions could be inferred/suggested:

$$v_1(x,y;t)=\frac{\sinh\left[k(b\ y)\right]}{\sinh\left[k(b\ a)\right]}\left(m_1\gamma_1'(t)+\left(\frac{\alpha_{12}m_1}{\rho_1}+ikV_1\right)\gamma_1(t)\right)e^{ikx}+c.c., \tag{18}$$

$$v_2(x,y;t)=\frac{1}{\sinh(2ak)}\left[\sinh\left[k(a+y)\right]\left(m_2\gamma_1'(t)+\left(\frac{\alpha_{12}m_2}{\rho_2}+ikV_2\right)\gamma_1(t)\right)\right.$$
$$\left.+\sinh\left[k(a-y)\right]\left(m_2\gamma_2'(t)+\left(\frac{\alpha_{23}m_2}{\rho_2}+ikV_2\right)\gamma_2(t)\right)\right]e^{ikx}+c.c., \tag{19}$$

$$v_3(x,y;t)=\frac{\sinh\left[k(b+y)\right]}{\sinh\left[k(b-a)\right]}\left(m_3\gamma_2'(t)+\left(\frac{\alpha_{23}m_3}{\rho_3}+ikV_3\right)\gamma_2(t)\right)e^{ikx}+c.c., \tag{20}$$

$$P_1^{(1)}=\frac{\cosh\left[k(b-y)\right]}{k\ m_1^2\rho_1\sinh\left[k(b-a)\right]}\left[(\alpha_{12}m_1+ikV_1\rho_1)(\upsilon_1m_1+ikV_1\rho_1)\gamma_1(t)\right.$$
$$\left.+m_1\rho_1((\alpha_{12}+\upsilon_1)m_1+2ikV_1\rho_1)\gamma_1'(t)+m_1^2\rho_1^2\gamma_1''(t)\right]e^{ikx}, \tag{21}$$

$$P_1^{(2)}=\frac{1}{k\ m_2^2\rho_2\sinh(2ak)}\left[\cosh\left[k(a-y)\right]((\alpha_{23}m_2+ikV_2\rho_2)(\upsilon_2m_2+ikV_2\rho_2)\gamma_2(t)\right.$$
$$+m_2\rho_2((\alpha_{23}+\upsilon_2)m_2+2ikV_2\rho_2)\gamma_2'(t)+m_2^2\rho_2^2\gamma_2''(t)))$$
$$-\cosh\left[k(a+y)\right]((\alpha_{12}m_2+ikV_2\rho_2)(\upsilon_2m_2+ikV_2\rho_2)\gamma_1(t)+m_2\rho_2((\alpha_{12}+\upsilon_2)\ m_2$$
$$\left.+2ikV_2\rho_2)\gamma_1'(t)+m_2^2\rho_2^2\gamma_1''(t))\right]e^{ikx}, \tag{22}$$

and

$$P_1^{(3)}=\frac{-\cosh\left[k(b+y)\right]}{k\ m_3^2\rho_3\sinh\left[k(b-a)\right]}\left[(\alpha_{23}m_3+ikV_3\rho_3)(\upsilon_3m_3+ikV_3\rho_3)\gamma_2(t)\right.$$
$$\left.+m_3\rho_3((\alpha_{23}+\upsilon_3)m_3+2ikV_3\rho_3)\gamma_2'(t)+m_3^2\rho_3^2\gamma_2''(t)\right]e^{ikx}. \tag{23}$$

It should be noted that in the absence of the porous media ($m_j\to 1$ and $\nu_j\to 0$), the above equations tend to be early obtained by Moatimid.[19]

For the magnetic path:

According to Melcher,[35] the following conditions must be satisfied.

The tangential component of the magnetic potential vanishes at the rigid boundaries, this means that

$$\frac{\partial\psi_1}{\partial x}=0\quad\text{at}\quad y=b \tag{24}$$

and

$$\frac{\partial \psi_3}{\partial x} = 0 \quad \text{at} \quad y = -b. \tag{25}$$

- The Maxwell's conditions of the magnetic potential, where there are surface currents present at the interfaces, resulted in
  - The continuity of the normal component of the magnetic displacement of the plane interface is

$$\underline{\hat{n}}_l.(\mu_l H_l - \mu_{l+1} H_{l+1}) = 0, \quad l = 1, 2, \quad y = (-)^{l+1} a + \xi_l. \tag{26}$$

  - The discontinuity of the tangential magnetic field components in the interface requires

$$\underline{\hat{n}}_l \times (H_l - H_{l+1}) = \underline{J}_{f_l}, \quad l = 1, 2, \quad y = (-)^{l+1} a + \xi_l. \tag{27}$$

Applying the foregoing boundary conditions to the general solution as given in Equation (14), the following can be concluded:

$$\psi_1(x, y; t) = \frac{i}{\varepsilon^*} \sinh\left[k(b - y)\right] \times \left\{ \frac{\left[(\mu_1 H_1 - \mu_2 H_2)((\mu_2 - \mu_3)\sinh\left[k(3a - b)\right] - (\mu_2 + \mu_3)\sinh\left[k(a + b)\right])\right]}{+2\mu_2(\mu_2 H_2 - \mu_3 H_3)\sinh\left[k(a - b)\right]\gamma_2(t)} \right\} \times \cos \omega t e^{ikx} + c.c., \tag{28}$$

$$\psi_2(x, y; t) = \frac{i}{\varepsilon^*} \sinh[k(b - a)] \left\{ \begin{array}{l} [(\mu_1 H_1 - \mu_2 H_2)((\mu_2 - \mu_3)\sinh[k(2a - b + y)] \\ \quad - (\mu_2 + \mu_3)\sinh[k(b + y)])]\gamma_1(t) - \\ [(\mu_2 H_2 - \mu_3 H_3)((\mu_1 - \mu_2)\sinh[k(2a - b - y)] \\ \quad + (\mu_1 + \mu_2)\sinh[k(b - y)]]\gamma_2(t)) \end{array} \right\} \cos \omega t e^{ikx} + c.c.\,, \tag{29}$$

and

$$\psi_3(x, y; t) = \frac{i}{\varepsilon^*} \sinh[k(b + y)] \left\{ \begin{array}{l} 2\mu_2(\mu_1 H_1 - \mu_2 H_2)\sinh\left[k(a - b)\right]\ \gamma_1(t) \\ \quad - [(\mu_2 H_2 - \mu_3 H_3)((\mu_1 - \mu_2)\sinh\left[k(3a - b)\right] \\ \quad + (\mu_1 + \mu_2)\sinh\left[k(a + b)\right]]\gamma_2(t) \end{array} \right\} \cos \omega t e^{ikx} + c.c., \tag{30}$$

where ε^* is given by

$$\varepsilon^* = \mu_2(\mu_1 + \mu_3)\cosh(2ak)\sinh[2k(a-b)] + \left(\mu_2^2 - \mu_1\mu_3\right)\sinh(2ak) - \left(\mu_2^2 + \mu_1\mu_3\right)\cosh[2k(a-b)]\sinh(2ak).$$

It should be noted that, in the absence of the periodicity of the magnetic field ($\omega \to 0$), the above equations are similar to those obtained by AlHamdan and Alkharashi.[31]

Now, the boundary-value problem has been completed. To proceed in light of linear stability analysis, a remaining boundary condition must be present. As stated previously, in view of the viscous potential theory, the viscous terms will appear only throughout the equation of the normal stress tensor, which is eliminated from the linear conservation of momentum. At the separation surface, the component of the total normal stress is discontinuous by the amount of the surface tension. The total stress tensor of the system under investigation is defined as

$$\sigma_{ij} = \sigma_{ij}^{\text{vis}} + \sigma_{ij}^{\text{mag}}, \tag{31}$$

where σ_{ij}^{vis} is the viscous stress tensor and σ_{ij}^{mag} is the Maxwell magnetic stress.

These stresses may be formulated as follows:

A large number of partially important fluids (eg, water and oil) are incompressible and exhibit a linear relation between the shear rate and strain, which are well known as the Newtonian fluids and their constitutive equation is given by

$$\sigma_{ij}^{\text{vis}} = -P\delta_{ij} + \eta\left(\frac{\partial v_i}{\partial x_j} + \frac{\partial v_j}{\partial x_i}\right), \tag{32}$$

where P is the pressure in the fluid and δ_{ij} is the Kronecker delta.

It is worthwhile to mention that, there are also many fluids which did not behave as the Newtonian fluids and have different constitutive equations, for example, toothpaste.

The magnetostatics and hydrodynamics are coupled together through the total stress tensor. In vacuum, the Coulomb force density exerted on free charges can be recorded taking into account the solenoid nature of the magnetostatic field. Furthermore, the derivation of the Maxwell stress tensor for a magnetic permeability medium is illustrated, in detail, by Melcher[35]

$$\sigma_{ij}^{\text{mag}} = \mu H_i H_j - \frac{1}{2}\mu H^2\delta_{ij}. \tag{33}$$

The derivation of the required dispersion relations will be derived in the next section.

3 | DERIVATION OF THE DISPERSION EQUATIONS

The components of the total force per unit area, exerted on the fluid interface, are related to components of the stress tensor via the following relation:

$$\underline{F} = \begin{pmatrix} \sigma_{xx} & \sigma_{xy} \\ \sigma_{yx} & \sigma_{yy} \end{pmatrix}\begin{pmatrix} n_x \\ n_y \end{pmatrix}, \tag{34}$$

where σ_{xx}, σ_{xy}, σ_{yy}, n_x, and n_y are the components of the stress tensor and unit normal to the interface, respectively.

At the fluid interfaces, the normal component of the stress tensor is discontinuous by the surface tension value. This requires

$$\hat{\underline{n}}\cdot\|\underline{F}\| = \chi_{l\,(l+1)}\,\nabla^2 S_l, \quad l = 1, 2, \tag{35}$$

where $\chi_{l(l+1)}$ is the surface tension coefficient of the surfaces that separate fluid l from fluid $l+1$. Substituting from the solutions of $\psi_1^{(j)}$, $v_1^{(j)}$, and $P_1^{(j)}$ $(j = 1, 2, 3)$ into the normal stress conditions (35) and considering $H_0^{(1)} = h_1 H_0$, $H_0^{(2)} = h_2 H_0$, and $H_0^{(3)} = h_3 H_0$ where $h_1 \neq h_2 \neq h_3$, after lengthy but straightforward calculations, one obtains the following coupled second-order linear differential equations

$$\begin{aligned} &f_{11}\gamma_1''(t) + f_{22}\gamma_2''(t) + (l_{11} + ig_{11})\gamma_1'(t) + (l_{22} + ig_{22})\gamma_2'(t) + (a_{11} + H_0^2\cos^2(\omega t)b_{11} + ic_{11})\gamma_1(t) \\ &\quad + (a_{22} + H_0^2\cos^2(\omega t)\,b_{22} + ic_{22})\,\gamma_2(t) = 0 \end{aligned} \tag{36}$$

and

$$\begin{aligned} &f_{22}\gamma_1''(t) + f_{12}\gamma_2''(t) + (l_{21} + ig_{22})\gamma_1'(t) + (l_{12} + ig_{12})\gamma_2'(t) + \left(a_{21} + H_0^2\cos^2(\omega t)\,b_{21} + i\,c_{21}\right)\gamma_1(t) \\ &\quad + \left(a_{12} + H_0^2\cos^2(\omega t)\,b_{12} + i\,c_{12}\right)\gamma_2(t) = 0, \end{aligned} \tag{37}$$

where the coefficients $f_{i\,l}$, $l_{i\,l}$, $g_{i\,l}$, $a_{i\,l}$, $b_{i\,l}$, and $c_{i\,l}$ are given in the Appendix A.

The amplitude of the elevation $\gamma_1(t)$ and $\gamma_2(t)$ are time-dependent functions of time, which determine the eigenvalue functions. The behavior of these functions governs the stability behavior of the fluid sheet. To facilitate the following analysis, only the symmetric and antisymmetric modes are considered.

3.1 | The symmetric and antisymmetric modes

The coupled second-order linear differential equations (36) and (37) can be simplified by considering the symmetric and antisymmetric deformations of the surface deflections ξ_1 and ξ_2. Therefore, in view of this concept, the variables ξ_1 and ξ_2 may be described by

$$\xi_2 = J\xi_1 = \xi, \tag{38}$$

where the symmetric deformation $J = -1$, and simultaneously $J = 1$, referring to the antisymmetric one. Considering the transformation (38) in the characteristic equations (36) and (37), it can be concluded that

$$\gamma''(t) + (a_1 + ib_1)\,\gamma''(t) + \left(c_1 + H_0^2\cos^2(\omega t)\,d_1 + il_1\right)\gamma(t) = 0 \tag{39}$$

and

$$\gamma''(t) + (a_2 + ib_2)\,\gamma'(t) + \left(c_2 + H_0^2\cos^2[\omega t]\,d_2 + il_2\right)\gamma(t) = 0, \tag{40}$$

where the coefficients a_l, b_l, c_l, d_l, and l_l are listed in the Appendix A.

The coupled differential equations (39) and (40) may be combined by adding them to give a single dispersion equation as

$$\gamma''(t) + (A + iB)\,\gamma''(t) + \left(C + H_0^2\cos^2(\omega t)\,D + iL\right)\gamma(t) = 0, \tag{41}$$

where the coefficients A, B, C, and D are given as follows:

$$A = (a_1 + a_2)/2, \quad B = (b_1 + b_2)/2, \quad C = (c_1 + c_2)/2, \quad D = (d_1 + d_2)/2,$$

and

$$L = (l_1 + l_2)/2.$$

The following section is devoted to analyzing the stability analysis in the previous case.

4 | STABILITY ANALYSIS IN THE PRESENCE OF A UNIFORM MAGNETIC FIELD

For a uniform tangential magnetic field, the periodicity of the field will be disappeared. Therefore, the previous dispersion equation, Equation (41), can be written as

$$\gamma''(t) + (A + iB)\gamma'(t) + (C + H_0^2 D + iL)\gamma(t) = 0. \tag{42}$$

Equation (42) is a linear homogeneous second-order differential equation with complex coefficients.

Since the amplitude of the surface wave $\gamma(t)$ is a real function, one may separate the real and imaginary parts to get

$$\gamma''(t) + A\gamma'(t) + \left(C + H_0^2 D\right)\gamma(t) = 0 \tag{43}$$

and

$$B\gamma'(t) + L\gamma(t) = 0. \tag{44}$$

Combining Equations (43) and (44), one gets

$$\gamma''(t) + \left(C - A\,L/B + H_0^2 D\right)\gamma(t) = 0. \tag{45}$$

Equation (45) is a linear homogeneous second-order differential equation; therefore, it may have an exponential solution. It follows that the solution of the dispersion equation (45), may be written as

$$\gamma(t) = \gamma_0 e^{i\Omega t}, \tag{46}$$

where γ_0 is some finite constant, and Ω is another constant which determines the natural frequency of the surface wave. From Equations (45) and (46), one finds

$$\Omega^2 - \left(C - AL/B + H_0^2 D\right) = 0. \tag{47}$$

Equation (47) represents a linear dispersion relation for the double interfaces that propagate through the magnified streaming sheet in permeable media. This dispersion relation is satisfied by the estimations of Ω, which is so-called the natural frequency, and k. The necessary criterion of stability may be represented as

$$DH_0^2 + \beta > 0, \tag{48}$$

where the coefficient β is given by $\beta = C - AL/B$.

The influence of the magnetic field on stability depends mainly on the sign of the parameter D. If $D > 0$, this implies that H_0^2 has a stabilizing influence and vice versa.

Lately, it has become convenient to depict the stability picture of the magnetic field intensity H_0^2 vs the wave number of the surface waves k. In fact, the parameter D depends on k. Consequently, the implication of the sign of the parameter D needs that the domain of the function $H_0^2 = H_0^2(k)$ must depend on this behavior.

Before dealing with a numerical calculation, it is required to rewrite the stability criterion in a convenient nondimensional form. This procedure depends mainly on the choice of some characteristics. For this purpose, consider the characteristic length b, the characteristic time $\sqrt{b/g}$, and the characteristic mass $\eta_2 b\sqrt{b/g}$. The other nondimensional quantities are given by the following:

$$k = \frac{k^*}{b},\ a = a^*\, b,\ \rho = \rho^* \frac{\eta_2}{b}\sqrt{1/bg},\ \chi_{l(l+1)} = \chi^*_{l(l+1)}\, \eta_2 \sqrt{bg},$$
$$\alpha_{l(l+1)} = \alpha^*_{l(l+1)} \frac{\eta_2}{b^2},\ \nu = \nu^* \frac{\eta_2}{b^2},\ \eta = \eta^*\, \eta_2,\ \text{and } H_0^2 = H_0^{*2} \eta_2 \sqrt{g/b}\ .$$

Generally, the attention was focused on the relationship between the magnetic field intensity log H_0^2 and the wave number of the surface wave k. Therefore, the stability diagram were depicted as log H_0^2 vs k. In the following figures, the stable region is denoted by the letter S. Simultaneously, the letter U stands for the unstable one. All the coming figures depict the stability criterion that is given by Equation (48). In these figures, the parameter D is always positive; this means that the tangential uniform magnetic field has a stabilizing effect. It should be noted that this is an early result, which was confirmed by many authors; for instance, see Zelazo and Melcher.[9] This shed light on exploring the effect of the various parameters on the stability configuration. The following figures show the case of antisymmetric mode.

Figure 2 was displayed to indicate the influence of the sheet thickness on the stability behavior. This figure represents a system having the following particulars:

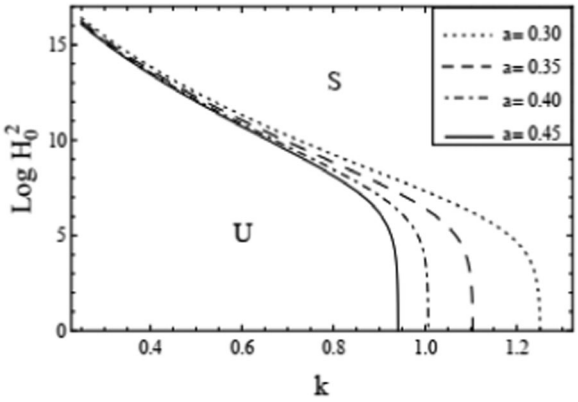

FIGURE 2 Plots of the stability bound for $\log H_0^2$ vs k for different values the parameter a for the mode $J = 1$

$$\rho_1 = 0.001, \quad \rho_2 = 0.01, \quad \rho_3 = 0.1, \quad m_1 = 0.12, \quad m_2 = 0.03, m_3 = 0.6,$$
$$V_1 = 15, \quad V_2 = 10, \quad V_3 = 5, \quad \mu_1 = 20, \quad \mu_2 = 30, \ \mu_3 = 10,$$
$$\eta_1 = 2.5, \quad \eta_3 = 4, \quad h_1 = 0.5, \quad h_2 = 0.3, \quad h_3 = 12, \quad \chi_{12} = 10,$$
$$\chi_{23} = 15, \quad \nu_1 = 10, \quad \nu_2 = 12, \quad \nu_3 = 7, \quad \alpha_{23} = 1, \alpha_{12} = 3.$$

As seen from this figure, it is clear that the increase of the sheet thickness leads to an increase in the stable region; this mechanism is enhanced at large values of the wave number. This shows a stabilizing influence of this parameter for the selected input parameters. The calculations presented thus far enable us to understand the role of the fluid dynamics on the instability of the problem. Similar results were obtained earlier by El-Shehawey et al.[4] Furthermore, this is in agreement with the results that were obtained by El-Dib and Matoog.[7]

The antisymmetric mode is pictured in Figure 3 to display the influence of the mass and heat transfer parameter between the two-phase layers (1) and (2). This parameter is denoted by the symbol α_{12}. The system chosen here is the same as that in Figure 2, except $a = 0.3$. As seen from this figure, the unstable region is enhanced as the parameter α_{12} is increased, which shows a destabilizing influence of this parameter. The destabilizing region is enhanced with increasing wave number; nonetheless, this mechanism is in contrast with the parameter α_{23}.

As presented in Figure 4, the parameter α_{23} has a stabilizing influence; therefore, it can be concluded that the mass and heat transfer has a dual role in the stability picture; this result was previously obtained by Moatimid.[19]

Figure 5 shows the influence of Darcy's coefficient ν_1 for a system having the same particulars as given in Figure 2. In this figure, the solid curve shows the neutral stability of the value of the Darcy's coefficients $\nu_1 = 50$, the value $\nu_1 = 40$ represents the dot-dashed line, and the dashed curve describes the value $\nu_1 = 30$, while the dotted line indicates the case of $\nu_1 = 20$. It is shown that this parameter has a destabilizing influence on the stability configuration. Actually, this role depends on the structure of the media. Additionally, this behavior is enhanced at large values of the wave number.

In Figures 6 and 7, the solid curve is plotted at the value $\mu_3 = 20.0$. The value $\mu_3 = 16.0$ corresponds to the dot-dashed line, and the dashed curve represents the value $\mu_3 = 12.0$, while the value $\mu_3 = 08.0$ depicts the dotted curve. Inspection of Figure 6 shows that this parameter

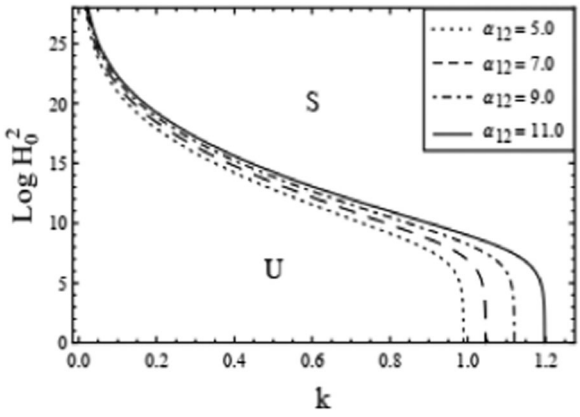

FIGURE 3 Plots of the stability bound for log H_0^2 vs k for different values of the parameter α_{12} at the mode $J = 1$

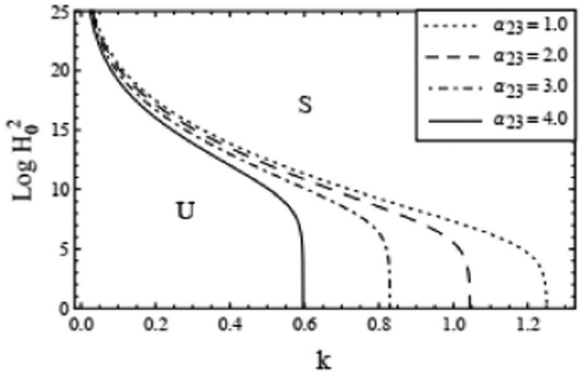

FIGURE 4 Plots of the stability bound for log H_0^2 vs k for different values of the parameter α_{23} at the mode $J = 1$

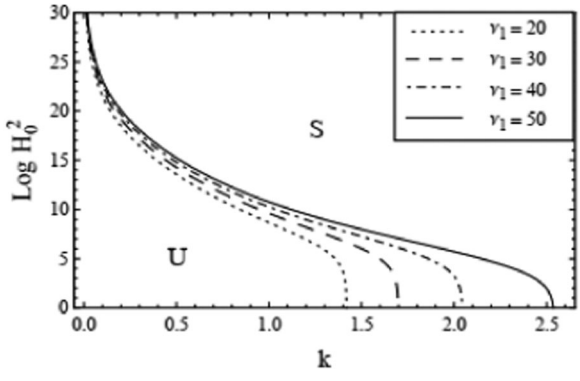

FIGURE 5 Plots of the stability bound for log H_0^2 vs k for different values of the parameter ν_1 at the mode $J = 1$

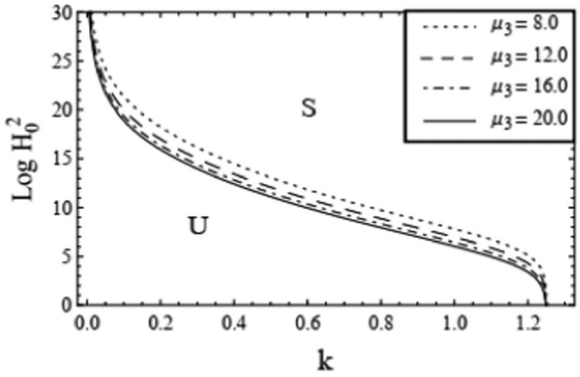

FIGURE 6 Plots of the stability bound for log H_0^2 vs k for different values of the parameter μ_3 at the mode $J = 1$

has a stabilizing effect. Furthermore, the system is completely stable for all values of the wave number as $k > 1.22$. Keep in mind that this figure represents the case of $J = 1$. The same behavior was seen in the case of $J = -1$. This was observed in Figure 7. In the later case, the transition curves change their behavior. As seen, the system is always stable for large values of the wave number. Therefore, it is concluded that the magnetic permeability of the third medium effect has a stabilizing influence on the stability picture. The same results were approved by Alkharashi.[12]

In Figure 8, the solid curve is plotted at the value $m_1 = 0.8$, the value $m_1 = 0.7$ corresponds to the dot-dashed line, and the dashed curve represents the value $m_1 = 0.6$, while the value $m_1 = 0.5$ depicts to the dotted curve. This figure indicates the stabilizing influence of the porosity of the antisymmetric mode ($J = 1$). This may occur due to the presence of the porous term in the governing equation of motion as given in Equation (4). Actually, the porosity acts as a drag force. Therefore, it reduces the instability of the system. The same mechanism occurs in the case of the symmetric mode ($J = -1$). Therefore, Figure 9 was plotted. Therefore, the porosity of the first layer always plays a stabilizing role in the stability picture in these modes of perturbation of the surface waves.

Figure 10 was plotted to indicate the influence of the change of the first fluid viscosity η_1 on the stability picture, where the values 6, 7, 8, and 9 are chosen for the quantity η_1. The inspection of Figure 10 reveals that the increasing of the viscosity ratio η_1 enhances the stability regions. As seen from this curve, for some value of the parameter η_1, the system is completely stable. This was an early result—it has been confirmed by many researchers; for instance, see Alkharashi et al.[12]

Figure 11 describes the influence of of the first fluid velocity V_1 in the stability picture. In this figure, the solid curve is plotted at the value $V_1 = 20$, the value $V_1 = 15$ corresponds to the dot-dashed line, and the dashed curve represents the value $V_1 = 10$, while the value $V_1 = 5$ depicts the dotted curve. It was shown that the destabilizing region increasing with the increasing of the velocity parameter. This indicated that velocity parameter has destabilizing influence, this according to Awasthi[36] and Moatimid et al.[8]

5 | STABILITY ANALYSIS OF THE PERIODIC MAGNETIC FIELD

To avoid repetition of the calculations, as given in Equations (42), (43), and (44), the dispersion equation in the present case may be written as follows:

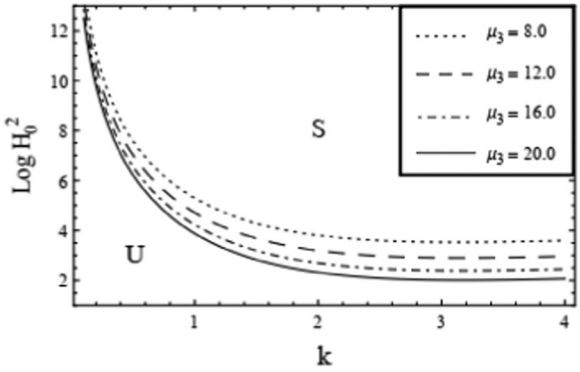

FIGURE 7 Plots of the stability bound for $\log H_0^2$ vs k for different values of the parameter μ_3 at the mode $J = -1$

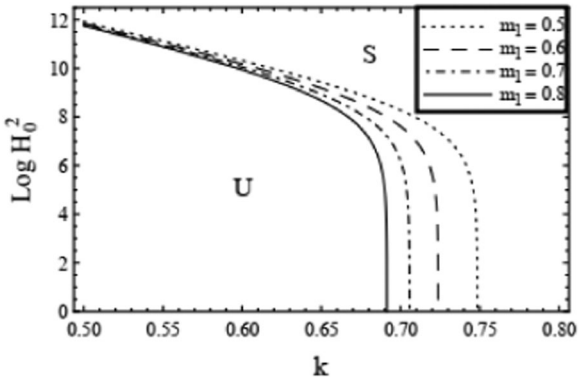

FIGURE 8 Plots of the stability bound for $\log H_0^2$ vs k for different values of the parameter m_1 at the mode $J = 1$

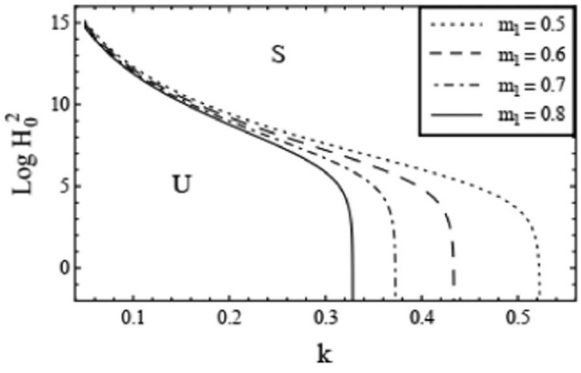

FIGURE 9 Plot of the stability bound for $\log H_0^2$ vs k for different values of the parameter m_1 at the mode $J = -1$

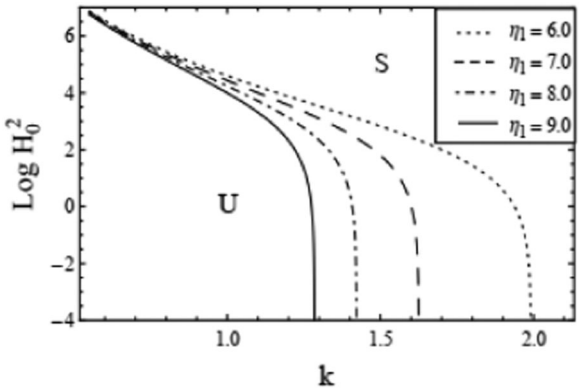

FIGURE 10 Plots of the stability bound for log H_0^2 vs k for different values of the parameter η_1 at the mode $J = 1$

$$\gamma'' + \left(C - LA/B + H_0^2 \cos^2(\omega t)\, D\right)\gamma(t) = 0. \tag{49}$$

A small parameter ε can be used to determine the transition curves, which separate the stable from unstable regions, according to Floquet theory.[37] Typically, on the homotopy perturbation method, one may choose a small parameter ε, such that $\varepsilon \in [0,\ 1]$. Equation (49) may be written as

$$\frac{d^2\gamma}{d\tau^2} + (\delta - \ \varepsilon\hat{q}\cos 2\tau)\gamma = 0, \tag{50}$$

where $\tau = \omega\ \ t$ is used, $\delta = (1/\omega^2)(C - LA/B + (1/2)DH_0^2)$, and $\hat{q} = -DH_0^2/2\omega^2$.

Equation (49) is the standard Mathieu differential equation. Both the characteristics and the applications of the Mathieu functions were investigated in the McLachlan' book.[37] The solutions of the Mathieu equation can be, in terms of certain considerations, periodic and the system is then stable. Moreover, the relationship between the parameters δ and $\hat{q}$ is considered the basis for the adoption of a requirement for obtaining a periodic Mathieu function. To study

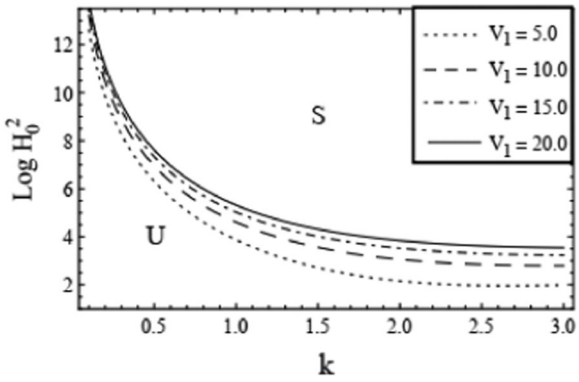

FIGURE 11 Graph of the stability bound for log H_0^2 vs k for the parameter V_1 at the mode the mode $J = -1$

the stability of Equation (50), a simple perturbation technique was used to obtain the transition curves, which separate the stability from instability regions.

An approximate solution to (50) is explored, by expanding γ and δ as follows:

$$\gamma(\tau,\varepsilon) = \gamma_0 + \varepsilon\gamma_1 + \varepsilon^2\gamma_2 + \varepsilon^3\gamma_3 + \cdots \tag{51}$$

and

$$\delta(\tau,\varepsilon) = n^2 + \varepsilon\delta_1 + \varepsilon^2\delta_2 + \varepsilon^3\delta_3 + \cdots, \tag{52}$$

where n is a nonnegative integer. Substituting Equations (51) and (52) into Equation (50) and equating coefficients of equal powers of ε, one finds

$$\frac{d^2\gamma_0}{d\tau^2} + n^2\gamma_0 = 0, \tag{53}$$

$$\frac{d^2\gamma_1}{d\tau^2} + n^2\gamma_1 = -(\delta_1 - \hat{q}\cos 2\tau)\gamma_0, \tag{54}$$

$$\frac{d^2\gamma_2}{d\tau^2} + n^2\gamma_2 = -(\delta_1 - \hat{q}\cos 2\tau)\,\gamma_1 - \delta_2\,\gamma_0, \tag{55}$$

and

$$\frac{d^2\gamma_3}{d\tau^2} + n^2\,\gamma_3 = -(\delta_1 - \hat{q}\cos 2\tau)\,\gamma_2 - \delta_2\,\gamma_1 - \delta_3\,\gamma_0. \tag{56}$$

The solution of the zero-order equation (53) may be represented as

$$\gamma_0 = \{\cos n\tau,\ \sin n\tau\}. \tag{57}$$

In the following, the higher approximation for the cases $n = 0,\ 1,\ 2,\ 3$ was determined.

5.1 | The case of $n = 0$

The bounded solution of Equation (57) gives

$$\gamma_0 = 1. \tag{58}$$

Therefore, Equation (54) becomes

$$\frac{d^2\gamma_1}{d\tau^2} = -(\delta_1 - \hat{q}\cos 2\tau). \tag{59}$$

To make γ_1 periodic, $\delta_1 = 0$ must be added; therefore, one gets

$$\gamma_1 = -\frac{1}{4}\hat{q}\cos 2\tau. \tag{60}$$

After substituting γ_0, γ_1, and δ_1 into Equation (55), it takes the following form:

$$\frac{d^2\gamma_2}{d\tau^2} = -\left(\delta_2 + \frac{1}{8}\hat{q}^2\right) - \frac{1}{8}\hat{q}^2\cos 4\tau. \tag{61}$$

To make γ_2 periodic, there must be

$$\delta_2 = -\hat{q}^2/8. \tag{62}$$

Hence, the second-order solution γ_2 becomes

$$\gamma_2 = \frac{1}{128}\hat{q}^2\cos 4\tau. \tag{63}$$

After substituting γ_0, γ_1, γ_2 , δ_1, and δ_2 into Equation (56), the following form was obtained:

$$\frac{d^2\gamma_3}{d\tau^2} = -\delta_3 - \frac{7}{256}\hat{q}^3\cos 2\tau + \frac{1}{256}\hat{q}^3\cos 6\tau. \tag{64}$$

It is concluded that $\delta_3 = 0$. Hence, the third-order solution γ_3 becomes

$$\gamma_3 = \frac{7}{1027}\hat{q}^3\cos 2\tau - \frac{1}{9216}\hat{q}^3\cos 6\tau. \tag{65}$$

Therefore, the transition curves separating stability from instability in the case of $n = 0$ being

$$\delta = -\frac{\hat{q}^2}{8}\varepsilon^2 + O(\varepsilon^3). \tag{66}$$

5.2 | The case of $n = 1$

The bounded solution of Equation (53) gives

$$\gamma_0 = c_1\cos\tau + c_2\sin\tau, \tag{67}$$

here c_1 and c_2 are the integration constants. Then (54) becomes

$$\frac{d^2\gamma_1}{d\tau^2} + \gamma_1 = c_1\left(\frac{1}{2}\hat{q} - \delta_1\right)\cos\tau - c_2\left(\frac{1}{2}\hat{q} + \delta_1\right)\sin\tau + \frac{\hat{q}}{2}(c_1\cos 3\tau + c_2\sin 3\tau). \tag{68}$$

To make γ_1 periodic, the secular terms must be removed. Consequently, one gets

$$\delta_1 = \pm\frac{\hat{q}}{2}. \tag{69}$$

Then the solution of (68) can be written as

$$\gamma_1 = c_3\cos\tau + c_4\sin\tau - \frac{\hat{q}}{16}(c_1\cos 3\tau + c_2\sin 3\tau), \tag{70}$$

where c_3 and c_4 are the integration constants.

After substituting γ_0, γ_1, and δ_1 into Equation (55), the following form was obtained:

$$\begin{aligned}\frac{d^2\gamma_2}{d\tau^2} + \gamma_2 = &\left[c_3\left(\frac{\hat{q}}{2} - \delta_1\right) - c_1\left(\frac{\hat{q}^2}{32} + \delta_2\right)\right]\cos\tau + \left[-c_2\left(\frac{\hat{q}^2}{32} + \delta_2\right) - c_4\left(\frac{\hat{q}}{2} + \delta_1\right)\right]\sin\tau\\ &+ \left[\frac{1}{16}\hat{q}c_1\delta_1 + \frac{1}{2}\hat{q}c_3\right]\cos 3\tau + \left[\frac{1}{16}\hat{q}c_2\delta_1 + \frac{1}{2}\hat{q}c_4\right]\sin 3\tau\\ &- \frac{1}{32}\hat{q}^2[c_1\cos 5\tau + c_2\sin 5\tau].\end{aligned} \tag{71}$$

To make γ_2 periodic, the secular terms must be neglected. So, it is concluded from (71) that

$$\delta_2 = -\frac{\hat{q}^2}{32}. \tag{72}$$

Then the second-order solution γ_2 of (71), after neglect its secular term, can be written as

$$\begin{aligned}\gamma_2 = &c_5\cos\tau + c_6\sin\tau - \frac{1}{16}\hat{q}\left[\frac{1}{8}c_1\delta_1 + c_3\right]\cos 3\tau - \frac{1}{16}\hat{q}\left[\frac{1}{8}c_2\delta_1 + c_4\right]\sin 3\tau\\ &+ \frac{1}{768}\hat{q}^2[c_1\cos 5\tau + c_2\sin 5\tau].\end{aligned} \tag{73}$$

After substituting of γ_0, γ_1, γ_2, δ_1, and δ_2 into Equation (56), it takes the following form:

$$\begin{aligned}\frac{d^2\gamma_3}{d\tau^2} + \gamma_3 = &\left[-c_1\left(\frac{1}{256}\hat{q}^2\delta_1 + \delta_3\right) + c_5\left(\frac{1}{2}\hat{q} - \delta_1\right)\right]\cos\tau\\ &- \left[c_2\left(\frac{1}{256}\hat{q}^2\delta_1 + \delta_3\right) + c_6\left(\frac{1}{2}\hat{q} + \delta_1\right)\right]\sin\tau + \frac{\hat{q}^3}{1536}[c_1\cos 7\tau + c_2\sin 7\tau]\\ &- \hat{q}^2\left[\frac{1}{192}c_1\delta_1 + \frac{1}{32}c_3\right]\cos 5\tau - \hat{q}^2\left[\frac{1}{192}c_2\delta_1 + \frac{1}{32}c_4\right]\sin 5\tau\\ &+ \left[\frac{1}{2}\hat{q}c_5 + \frac{1}{16}\hat{q}c_3\delta_1 + \frac{1}{1536}c_1\hat{q}^3\right]\cos 3\tau + \left[\frac{1}{2}\hat{q}c_6 + \frac{1}{16}\hat{q}c_4\delta_1 + \frac{1}{1536}c_2\hat{q}^3\right]\sin 3\tau.\end{aligned} \tag{74}$$

Then the third-order solution γ_3 of Equation (74), after neglect its secular term, can be written as

$$\gamma_3 = c_7 \cos\tau + c_8 \sin 7\tau - \frac{\hat{q}^3}{73728}[c_1 \cos 7\tau + c_2 \sin 7\tau] + \frac{1}{24}\hat{q}^2\left[\frac{1}{192}c_1\delta_1 + \frac{1}{32}c_3\right]\cos 5\tau + \frac{1}{24}\hat{q}^2\left[\frac{1}{192}c_2\delta_1 + \frac{1}{32}c_4\right]\sin 5\tau - \frac{1}{8}\left[\frac{1}{2}\hat{q}c_5 + \frac{1}{16}\hat{q}c_3\delta_1 + \frac{1}{1536}c_1\hat{q}^3\right]\cos 3\tau - \frac{1}{8}\left[\frac{1}{2}\hat{q}c_6 + \frac{1}{16}\hat{q}c_4\delta_1 + \frac{1}{1536}c_2\hat{q}^3\right]\sin 3\tau. \tag{75}$$

Similar to the previous technique, the following can be concluded

$$\delta_3 = -\frac{1}{512}\hat{q}^3. \tag{76}$$

One finds the transition curve separating stability from instability regions and emanating from $n = 1$ to be

$$\delta = 1 \pm \frac{\hat{q}}{2}\varepsilon - \frac{\hat{q}^2}{32}\varepsilon^2 - \frac{\hat{q}^3}{512}\varepsilon^3 + O(\varepsilon^4). \tag{77}$$

5.3 | The case of $n = 2$

The bounded solution of Equation (53) is given as

$$\gamma_0 = \tilde{c}_1 \cos 2\tau + \tilde{c}_2 \sin 2\tau, \tag{78}$$

where $\tilde{c}_1$ and $\tilde{c}_2$ are the integration constants.

Similar arguments as previously viewed may be utilized to obtain the following transition curves:

$$\delta = 4 - \frac{\hat{q}^2}{48}\varepsilon^2 + O(\varepsilon^4). \tag{79}$$

5.4 | The case of $n = 3$

The bounded solution of Equation (53) is given as

$$\gamma_0 = \hat{c}_1 \cos 3\,\tau + \hat{c}_2 \sin 3\tau, \tag{80}$$

where $\hat{c}_1$ and $\hat{c}_2$ are the integration constants.

One finds tha the transition curve separating stability from instability regions and emanating from $n = 3$ becomes

$$\delta = 9 + \frac{\hat{q}^2}{64}\varepsilon^2 \pm \frac{\hat{q}^3}{512}\varepsilon^3 + O(\varepsilon^4). \tag{81}$$

Taking the limit as $\varepsilon \to 1$, one can draw the obtained transition curves.

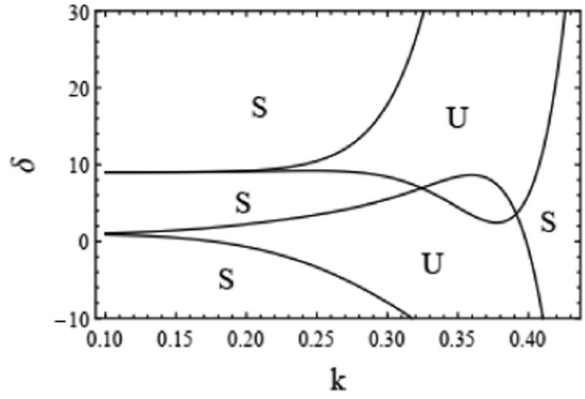

FIGURE 12 Plots the transition curves at $n = 1, 3$ bound for δ vs k at $J = 1$

In what follows, a sample of the transition curves will be plotted. For simplicity, the cases when $n = 1$ and 3 were chosen. Typically—as shown by many researchers; for instance, Nayfeh,[38] the region between the two transition curves gives the unstable region. Otherwise, the stable regions lie outside these curves; therefore, the following numerical discussions drawing the transition curves. These transition curves are represented by Equations (77) and (81) in the $\delta - k$ plane in case of antisymmetric mode, as well as the symmetric one, where $J = 1$ and $J = -1$, respectively. In the following figures, considering the previous nondimension quantities, a system having the following particulars were considered:

$$\rho_1 = 0.001,\ \rho_2 = 0.01,\ \rho_3 = 0.1,\ \mu_1 = 4,\ \mu_2 = 50,\ \mu_3 = 20,\ \eta_1 = 2.5,\ \eta_3 = 0.2,\ H_0^2 = 3,$$
$$\varepsilon = 1,\ \omega = 7,\ h_1 = 0.5,\ h_2 = 3, \text{and } h_3 = 0.2.$$

As presented in these figures, the transition curves are plotted for $n = 1,\ 3$. Therefore, the resonance modes had appeared due to the periodicity of the tangential magnetic field.

Figure 12 depicts the two transition curves. These curves portioned the plane $\delta - k$ into stable and unstable regions. This figure was plotted for the antisymmetric mode, where $J = 1$. As seen from this figure, away from the case of the uniform magnetic field, it is found that the stability

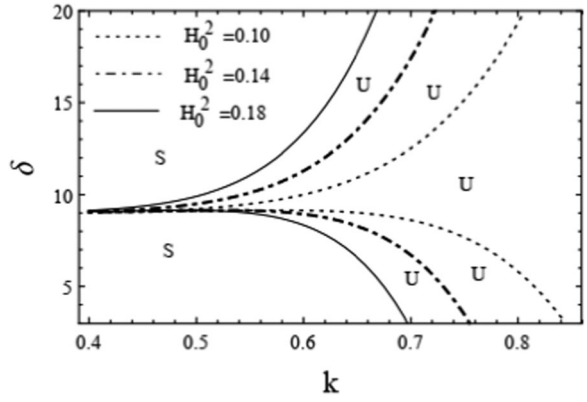

FIGURE 13 Plots of the transition curves at $n = 3$ bound δ vs k for different values of the magnetic field intensity at $J = 1$

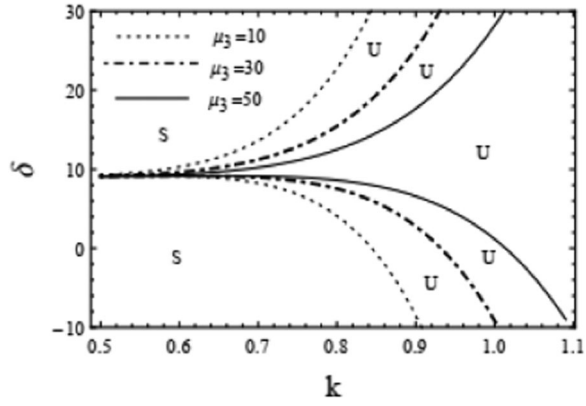

FIGURE 14 Graph of the transition curves at $n = 3$ bound δ vs k for different values of the magnetic permeability μ_3 at $J = 1$

diagram is portioned into several parts of stable and unstable regions. To indicate the influences of the different parameters in the stability picture, it is convenient to plot the transition curve at a certain n. Therefore, Figure 13 was depicted to indicate the influence of the magnetic field intensity on the transition curves at $n = 3$. As seen from this figure, the unstable region increases with the increasing of the magnetic field intensity H_0^2. This result agrees with the study of Alkharashi and Gamiel[25] in their studying about a periodic normal electric field. It is worthwhile to observe that this mechanism is in contrast with that seen in the case of the uniform magnetic field. Therefore, the magnetic field played a dual role in the stability profile.

Figures 14 and 15, the solid curve is plotted at the value $\mu_3 = 50$, and the value $\mu_3 = 30$ corresponds to the dot-dashed line, while the value $\mu_3 = 10$ depicts to the dotted curve. The system chosen here is the same as in Figure 12, except $a = 0.05$, $\mu_1 = 80$, $\mu_2 = 30$, $\omega = 2, H_0^2 = 0.1$, and $h_2 = 0.3$. Figure 14 was depicted to indicate the influence of the magnetic permeability of the third medium μ_3 on the stability picture. As seen from Figure 14, the unstable region decreases with the increasing of the magnetic permeability at antisymmetric mode $J = -1$. This shows a stabilizing influence of this parameter. Similar figure was plotted in the previous case, where the uniform field was

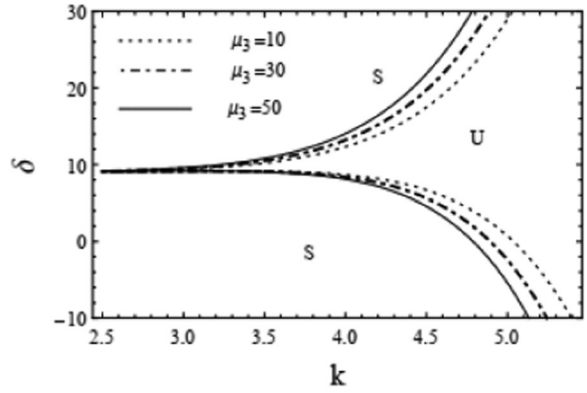

FIGURE 15 Plot of the transition curves at $n = 3$ bound δ vs k for different values of the magnetic permeability μ_3 at $J = -1$

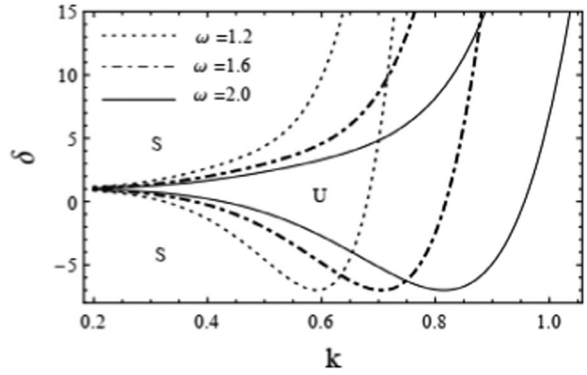

FIGURE 16 Graph of the transition curves at $n = 1$ bound δ vs k for different values of the magnetic field frequency at $J = 1$

affected. Figure 15 was plotted for the case of the symmetric mode as $J = 1$. In contrast with the previous case as $J = -1$, the unstable region is increased with the increase of this parameter. Therefore, the magnetic permeability has a destabilizing effect on the wave motion at symmetric mode due to the periodic magnetic field. This shows that the role of this parameter, depends on the mode of the surface wave. Similar results are previously obtained by Moatimid.[39]

Figure 16 was depicted to illustrate the influence of the frequency of the magnetic field for the transition curves at the resonance $n = 1$ of antisymmetric mode, where $J = 1$. The system chosen here is the same as in Figure 14 at $\mu_3 = 10$ with the variation of the magnetic field periodicity ω. As seen from this figure, the unstable region decreases with the increasing of the magnetic field frequency ω for all values of the wave number k. The same behavior was shown in Figure 17. The final figure was plotted for the case, where $n = 1$, and for symmetric mode, where $J = -1$. From these two figures, it was found that the increasing of the values of the magnetic field frequency ω increases the stable regions. This shows a stabilizing influence of the periodicity. Typically, this result was initially shown by several researchers (for instance, see El-Dib and Matoog[7]).

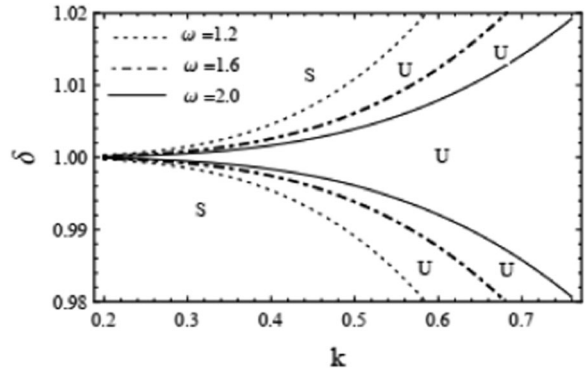

FIGURE 17 Graph of the transition curves at $n = 1$ bound δ vs k for different values of the magnetic field frequency at $J = -1$

6 | CONCLUDING REMARKS

In the present work, the ferrodynamic instability problem of double interfaces separated three incompressible viscous fluids was studied. The problem meets its significance from the geophysics point of view. In addition, the case of the separation of water from oil-water mixture depends mainly of the problem of two-phase fluids. The interfaces, in the current study, allowed a transfer of mass and heat. To relax the mathematical manipulation, the analysis followed a simplified formulation that was first established by Hsieh.[17,18] The transfer of the mass and heat across the interfaces was revealed throughout two parameters α_{12} and α_{23}. Undoubtedly, this formulation facilitated the complexity of the practical applications. The system was stressed upon by horizontal harmonic magnetic fields, of different strengths, which admitted the presence of free-surface currents. The analysis was undertaken principally by the coupling between these parameters. Typically, as other interface stability problems, the hydrodynamic equations and Maxwell equations were solved individually. Simultaneously, the interaction between the hydrodynamic and magnetic field occurred, only, throughout the stress balance across the interfaces; the simplified version of this problem was already performed by Moatimid.[19] Therefore, to avoid the length of the manuscript, the details of the derivations were ignored in the present manuscript. So, the analysis of the current problem seems hard to understand. Due to the vast importance of the practical applications of porous media, the attention here was focused on the porous media parameters and the viscous effects. To avoid the complexity of the mathematical analysis in considering the viscous effects, the viscous potential theory was utilized. The procedure resulted in coupled linear second-order differential equations of complex and periodic coefficients. To simplify the mathematical treatment, the symmetric and antisymmetric modes of perturbation were only considered. The stability analysis was theoretically discussed and the results were confirmed in the uniform as well as periodic magnetic field. The growth rate of the perturbation was also evaluated for the intensity of magnetic field vs the wave number of the surface waves. In case of the oscillating field, the transition curves were obtained. The numerical calculations, draw the following concluding remarks:

For uniform magnetic field:

In case of the antisymmetric mode ($J = 1$),

- The sheet thickness plays a stabilizing influence. This result was previously shown by El-Shehawey et al.[4]
- The mass and heat transfer play a dual role in the stability configuration. In other words, the parameter α_{12} has a destabilizing influence and vice versa for the parameter α_{23}. This behavior is shown previously by Moatimid.[19]
- Darcy's coefficient ν_1 has a destabilizing influence.
- Actually, the porosity acts as a drag force. Therefore, it has a stabilizing effect in the stability profile.
- The magnetic permeability μ_3 has a stabilizing effect.

In case of the symmetric mode ($J = -1$),

- The dynamic viscosity η_1 has a stabilizing influence.
- The magnetic permeability μ_3 has a stabilizing effect.
- The streaming V_1 has a destabilizing influence. This is an early result, which was shown by many other researchers.

For periodic magnetic field:

- The standard instability, the parametric instabilities caused by resonances between the surface waves and excited periodic magnetic field are obtained.
- Several transition curves are theoretically obtained.
- The numerical calculations show that, the magnetic permeability μ_3 has a dual effect in the stability picture. In other words, the magnetic permeability μ_3 has a stabilizing role in antisymmetric mode, and vice versa for symmetric mode.
- The periodicity of the magnetic field has a stabilizing influence.
- The magnetic field intensity plays a dual role in the stability picture. In other words, the uniform magnetic field has a stabilizing role, and vice versa for the periodic field.

ACKNOWLEDGMENTS

The authors appreciate the reviewers for their interest in the topic of the current work and their useful and valuable comments that improved the original manuscript.

ORCID

Aya Sayed http://orcid.org/0000-0002-5596-024X

REFERENCES

1. Rayleigh L. Investigation of the character of the equilibrium of an incompressible heavy fluid of variable density. *Proc London Math Soc*. 1883;14:170-177.
2. Taylor GI. The instability of liquid surfaces when accelerated in a direction perpendicular to their planes. *Proc Royal Soc London, A*. 1950;201(1056):192-196.
3. Chandrasekhar S. *Hydrodynamic and Hydromagnetic Stability*. Oxford, UK: Clarendon Press; 1961.
4. El-Shehawey SF, El-Dib YO, Mohamed AEMA. Electrohydrodynamic stability of a fluid layer: I.-Effect of a tangential field. *IL Nuovo Cimento D*. 1985;6(4):291-308.
5. Mohamed AEMA, El hehawey ESF, El Dib YO. Electrohydrodynamic stability of a fluid layer. Effect of a tangential periodic field. *Il Nuovo Cimento D*. 1986;8(2):177-192.
6. Mohamed AEMA, Shehawey ESFE, Dib YOE. Electrohydrodynamic stability of a fluid layer. II. Effect of a normal electric field. *J Chem Phys*. 1986;85:445-455.
7. El-Dib YO, Matoog RT. Stability of streaming in an electrified Maxwell fluid sheet influenced by a vertical periodic field in the absence of surface charges. *J Colloid Interface Sci*. 2000;229:29-52.
8. Moatimid GM, El-Dib YO, Zekry MH. Stability analysis using multiple scales homotopy approach of coupled cylindrical interfaces under the influence of periodic electrostatic fields. *Chin J Phys*. 2018;56:2507-2522.
9. Zelazo RE, Melcher JR. Dynamics and stability of ferrofluids: surface interaction. *J Fluid Mech*. 1969;39:1-24.
10. El-Dib YO. Nonlinear Rayleigh Taylor instability for hydromagnetic Darcian flow: effect of free surface currents. *J Colloid Interface Sci*. 2003;259:309-321.
11. Elhefnawy AR, Mahmoud MA, Mahmoud MA, Khedr GM. Nonlinear instability of two superposed magnetic fluids in porous media under vertical magnetic field. *Can Appl Math Q*. 2004;12(3):323-350.
12. Alkharashi SA. Dynamical system of three magnetic layers in the presence of porous media. *J Appl Math Phys*. 2015;03:310-321.
13. Horstmann GM, Wylega M, Weier T. Measurement of interfacial wave dynamics in orbitally shaken cylindrical containers using ultrasound pulse-echo techniques. *Exp Fluids*. 2019;60(4):56.
14. Wang Y. Sharp nonlinear stability criterion of viscous non-resistive MHD internal waves in 3D. *Arch Ration Mech Anal*. 2019;231:1675-1743.
15. Rohsenow WM. *Modern Developments in Heat Transfer*. New York, NY: Academic Press; 1963.

16. Leppert G, Pitts CC. *Advances in Heat Transfer*. New York, NY: Academic Press; 1964.
17. Hsieh DY. Effects of heat and mass transfer on Rayleigh-Taylor instability. *J Basic Eng*. 1972;94:156-160.
18. Hsieh DY. Interfacial stability with mass and heat transfer. *Phys Fluids*. 1978;21(5):745-748.
19. Moatimid GM. Stability conditions of an electrified miscible viscous fluid sheet. *J Colloid Interface Sci*. 2003;259(1):186-199.
20. Moatimid GM, Obied Allah MH, Hassan MA. Kelvin-Helmholtz instability for flow in porous media under the influence of oblique magnetic fields: a viscous potential flow analysis. *Phys Plasmas*. 2013;20:102111.
21. Awasthi MK. Electrohydrodynamic capillary instability with heat and mass transfer. *Ain Shams Eng J*. 2014;5:263-70.
22. El-Sayed MF, Moatimid GM, Metwaly TMN. Three dimensional nonlinear instability analysis of electroconvective finite dielectric fluids. *Int J Pure Appl Math*. 2018;118(4):895-920.
23. Bau HH. Kelvin-Helmholtz instability for parallel flow in porous media: a linear theory. *Phys Fluids*. 1982;25(10):1719-1722.
24. Zakaria K, A Sirwah M, Alkharashi S. Temporal stability of superposed magnetic fluids in porous media. *Physica Scripta*. 2008;77:025401.
25. Alkharashi SA, Gamiel Y. Stability characteristics of periodic streaming fluids in porous media. *Theor Math Phys*. 2017;191(1):580-601.
26. Moatimid GM, El-Dib YO, Zekry MH. Instability analysis of a streaming electrified cylindrical sheet through porous media. *Pramana*. 2019;92:22.
27. Stokes GG, Larmor J. On the effect of the internal friction of fluids on the motion of pendulums. *Math Phys Papers*. 1850;3:1880-1905.
28. Joseph DD. Potential flow of viscous fluids: historical notes. *Int J Multiph Flow*. 2006;32:285-310.
29. Sirwah MA. Nonlinear Kelvin–Helmholtz instability of magnetized surface waves on a subsonic gas–viscous potential liquid interface. *Physica A: Stat Mech Appl*. 2007;375(1,2):381-400.
30. Awasthi MK, Asthana R, Agrawal GS,. Viscous corrections for the viscous potential flow analysis of magnetohydrodynamic Kelvin-Helmholtz instability with heat and mass transfer. *Eur Phys J A*. 2012;48:174-183.
31. R. AlHamdan A, Alkharashi SA. Stability characterization of three porous layers model in the presence of transverse magnetic field. *J Math Res*. 2016;8(2):69-81.
32. Parekh K, Upadhyay RV. Characterization of transformer oil based magnetic fluid. *Indian J Eng Mater Sci*. 2004;11:262-266.
33. Yayla S, Ibrahim SS, Olcay AB. Numerical investigation of coalescing plate system to understand the separation of water and oil in water treatment plant of petroleum industry. *Eng Appl Comput Fluid Mech*. 2017;11(1):184-192.
34. Chakrabarti DP, Das G. Experimental studies on three-layer flow pattern in oil-wave horizontal flow. *Int J Transp Phenom*. 2012;13(1):1-14.
35. (a) Melcher JR. *Field Coupled Surface Waves*. Cambridge, MA: MIT Press; 1963; (b) Melcher JR. *Continuum Electromechanics*. Cambridge, MA: MIT Press; 1981.
36. Awasthi MK. Study on Kelvin–Helmholtz instability with heat and mass transfer. *J Fluids Eng*. 2014;136(12):121202.
37. McLachlan NW. *Theory and Application of Mathieu Functions*. Oxford, UK: Clarendon; 1964.
38. Nayfeh AH. *Problems in Perturbation*. New York, NY: Wiley; 1985.
39. Moatimid GM. The effect of a time harmonic-magnetic field on the stability of cylindrical ferrofluids in the presence of heat and mass transfer. *Can J Phys*. 1995;73:595-601.

How to cite this article: Moatimid GM, Eldabe NT, Sayed A. The effect of a periodic tangential magnetic field on the stability of a horizontal magnetic fluid sheet. *Heat Transfer—Asian Res*. 2019;1–31. https://doi.org/10.1002/htj.21583

APPENDIX A

Coefficients that were appearing in Equations (36) for $l = 1$ and (37) for $l = 2$ were listed as follows:

$$f_{1l} = \frac{1}{k}[\rho_{(2l-1)}\cosh(b-a)k\,\csc h(a-b)k - \rho_2\coth 2ak],$$

$$f_{22} = \frac{\rho_2}{k}\csc h(2ak),$$

$$g_{1l} = \frac{2\,V_{2l-1}\rho_{2l-1}}{m_{2l-1}}\coth(a-b)k - \frac{2\,V_2\rho_2}{m_2}\coth(2ak), \quad g_{22} = \frac{2\,V_2\rho_2}{m_2}\csc h(2ak),$$

$$l_{1l} = \frac{1}{2k}\csc h(2ak)\csc h((a-b)k)[\sinh(3a-b)k(\nu_{(2l-1)} - \nu_2 + 2k^2(m_{(2l-1)}\eta_{(2l-1)} - m_2\eta_2))$$
$$+ \sinh(a+b)k(2\alpha_{l(l+1)} + \nu_{2l-1} + \nu_2 + 2k^2(m_{2l-1}\eta_{2l-1} + m_2\eta_2)),$$

$$l_{2(3-l)} = \frac{1}{k}(\alpha_{(3-l)(4-l)} + \nu_2 + 2k^2m_2\eta_2)\csc h(2ak), \quad c_{2(3-l)} = \frac{kV_2}{m_2}h_{2(3-l)},$$

$$a_{2(3-l)} = \frac{\alpha_{(3-l)(4-l)}}{k\,\rho_2}\nu_2 + 2k^2m_2\,\eta_2\,\csc h(2ak) - \frac{k\rho_2\,V_2^2}{m_2^2}\csc h(2ak),$$

$$b_{2(3-l)} = \frac{2k\mu_2}{\mu^*}\sinh^2((a-b)k)(h_2\,\mu_2 - h_{(5-2l)}\mu_{(5-2l)})(h_2\,\mu_2 - h_{(2l-1)}\mu_{(2l-1)}),$$

$$b_{1l} = \frac{k}{\mu^*}(h_{(2l-1)}\mu_{(2l-1)} - h_2\,\mu_2)^2\sinh((b-a)k)[(\mu_2 - \mu_{(5-2l)})\sinh((3a-b)k)$$
$$- (\mu_2 + \mu_{(5-2l)})\sinh((a+b)k)],$$

$$\mu^* = -\cosh 2ak\,\sinh(2(a-b)k)\mu_2(\mu_{2l-1} + \mu_{(5-2l)}) + \sinh(2ak)(-\mu_2^2 + \mu_{(2l-1)}\mu_{(5-2l)})$$
$$+ \cosh(2(a-b)k)\sinh(2ak)(\mu_2^2 + \mu_{(2l-1)}\mu_{(5-2l)}),$$

$$a_{1l} = -k^2\chi_{l(l+1)} + g(\rho_l - \rho_{l+1})\frac{k\rho_2V_2^2}{m_2^2}\coth 2ak - \frac{k\rho_{2l-1}V_{(2l-1)}^2}{m_{(2l-1)}^2}\coth((a-b)k)$$
$$+ \frac{\alpha_{l(l+1)}}{k\rho_2\rho_{(2l-1)}}(-\rho_{2l-1}(\nu_2 + 2k^2m_2\eta_2)\coth(2ak) + \rho_2(\nu_{(2l-1)} + 2k^2m_{2l-1}\eta_{(2l-1)})$$
$$\coth((a-b)k)),$$

and

$$c_{1l} = \frac{1}{m_{(2l-1)}m_2}(m_2V_{(2l-1)}(\alpha_{l(l+1)} + \nu_{(2l-1)} + 2k^2m_{(2l-1)}\eta_{(2l-1)})\coth(a-b)k$$
$$- m_{(2l-1)}V_2(\alpha_{l(l+1)} + \nu_2 + 2k^2m_2\eta_2)\coth 2ak).$$

The coefficients that were appearing in the Equations (39) and (40) are listed as follows:

$$a_1 = \frac{l_{11} + Jl_{22}}{f_{11} + Jf_{22}}, \quad b_1 = \frac{g_{11} + Jg_{22}}{f_{11} + Jf_{22}}, \quad c_1 = \frac{a_{11} + Ja_{22}}{f_{11} + Jf_{22}}, \quad d_1 = \frac{b_{11} + Jb_{22}}{f_{11} + Jf_{22}}, l_1 = \frac{c_{11} + Jc_{22}}{f_{11} + Jf_{22}}$$

$$a_2 = \frac{l_{21} + Jl_{12}}{f_{22} + Jf_{12}}, \quad b_2 = \frac{g_{22} + Jg_{12}}{f_{22} + Jf_{12}}, \quad c_2 = \frac{a_{21} + Ja_{12}}{f_{22} + Jf_{12}}, \quad d_2 = \frac{b_{21} + Jb_{12}}{f_{22} + Jf_{12}},$$

and

$$l_2 = \frac{c_{21} + Jc_{12}}{f_{22} + Jf_{12}}$$